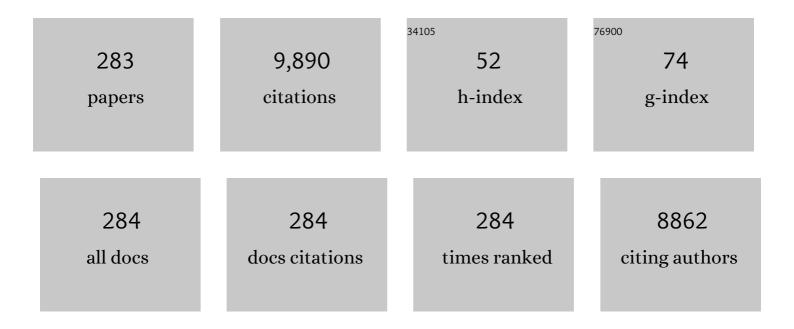
List of Publications by Year in descending order

Source: https://exaly.com/author-pdf/9577564/publications.pdf Version: 2024-02-01



ZHI DANC

#	Article	IF	CITATIONS
1	Environmental contamination and human exposure of polychlorinated biphenyls (PCBs) in China: A review. Science of the Total Environment, 2022, 805, 150270.	8.0	65
2	Synergistic removal of Cr(VI) by S-nZVI and organic acids: The enhanced electron selectivity and pH-dependent promotion mechanisms. Journal of Hazardous Materials, 2022, 423, 127240.	12.4	43
3	Inhibition of organosilane/ATP@HQ self-healing passivator for pyrite oxidation. Chemosphere, 2022, 287, 132342.	8.2	5
4	Rapid and efficient reduction of chromate by novel Pd/Fe@biomass derived from Enterococcus faecalis. Environmental Research, 2022, 204, 112005.	7.5	9
5	Twelve natural estrogens in urines of swine and cattle: Concentration profiles and importance of eight less-studied. Science of the Total Environment, 2022, 803, 150042.	8.0	17
6	A collaborative strategy for elevated reduction and immobilization of Cr(VI) using nano zero valent iron assisted by schwertmannite: Removal performance and mechanism. Journal of Hazardous Materials, 2022, 422, 126952.	12.4	24
7	Stability properties of natural estrogen conjugates in different aqueous samples at room temperature and tips for sample storage. Environmental Science and Pollution Research, 2022, 29, 24589-24598.	5.3	5
8	Efficient recovery of rare earth elements from discarded NdFeB magnets by mechanical activation coupled with acid leaching. Environmental Science and Pollution Research, 2022, 29, 25532-25543.	5.3	11
9	Degradation of organophosphorus flame retardants in heterogeneous photo-Fenton system driven by Fe(III)-based metal organic framework: Intermediates and their potential interference on bacterial metabolism. Chemosphere, 2022, 291, 133072.	8.2	14
10	Amino-functionalized MIL-88B as heterogeneous photo-Fenton catalysts for enhancing tris-(2-chloroisopropyl) phosphate (TCPP) degradation: Dual excitation pathways accelerate the conversion of FeIII to FeII under visible light irradiation. Journal of Hazardous Materials, 2022, 425, 127782.	12.4	24
11	Degradation of tris(2-chloroethyl) phosphate (TCEP) by thermally activated persulfate: Combination of experimental and theoretical study. Science of the Total Environment, 2022, 809, 152185.	8.0	15
12	17α-ethynylestradiol and its two main conjugates in seven municipal wastewater treatment plants: Analytical method, their occurrence, removal and risk evaluation. Science of the Total Environment, 2022, 812, 152489.	8.0	16
13	Effects of medical waste incineration fly ash on the promotion of heavy metal chlorination volatilization from incineration residues. Journal of Hazardous Materials, 2022, 425, 128037.	12.4	32
14	Mechanistic insights into the environmental fate of tetracycline affected by ferrihydrite: Adsorption versus degradation. Science of the Total Environment, 2022, 811, 152283.	8.0	20
15	Sulfite may disrupt estrogen homeostasis in human via inhibition of steroid arylsulfatase. Environmental Science and Pollution Research, 2022, 29, 19913.	5.3	2
16	Occurrence, spatial distribution, and main source identification of ten bisphenol analogues in the dry season of the Pearl River, South China. Environmental Science and Pollution Research, 2022, 29, 27352-27365.	5.3	20
17	Coupled Sorption and Oxidation of Soil Dissolved Organic Matter on Manganese Oxides: Nano/Sub-nanoscale Distribution and Molecular Transformation. Environmental Science & Technology, 2022, 56, 2783-2793.	10.0	34
18	Molecular-scale study of Cr(<scp>vi</scp>) adsorption onto lepidocrocite facets by EXAFS, <i>in situ</i> ATR-FTIR, theoretical frequency calculations and DFT+U techniques. Environmental Science: Nano, 2022, 9, 568-581.	4.3	6

#	Article	IF	CITATIONS
19	Assessing environmental fate of hexavalent chromium as influenced by fractionation of ferrihydrite with dissolved organic matter. Journal of Environmental Management, 2022, 306, 114489.	7.8	5
20	MgO-loaded nitrogen and phosphorus self-doped biochar: High-efficient adsorption of aquatic Cu2+, Cd2+, and Pb2+ and its remediation efficiency on heavy metal contaminated soil. Chemosphere, 2022, 294, 133733.	8.2	66
21	Investigation of the Interactions Occurring Between Cr(VI) and Citric Acid-Schwertmannite Composites: A Macroscopic and In Situ ATR-FTIR Study. ACS Earth and Space Chemistry, 2022, 6, 391-402.	2.7	5
22	Reduction of acid mine drainage by passivation of pyrite surfaces: A review. Science of the Total Environment, 2022, 832, 155116.	8.0	26
23	Activity measurement of arylsulfatase and βâ€glucuronidase in activated sludge: HPLCâ€based versus classical spectrophotometric method. Water Environment Research, 2022, 94, e10704.	2.7	3
24	Effect of polystyrene microplastics on the degradation of sulfamethazine: The role of persistent free radicals. Science of the Total Environment, 2022, 833, 155024.	8.0	19
25	17α-Estradiol, an ignored endogenous natural estrogen in human: Updated estrogen metabolism pathways and its environmental risk analysis. Science of the Total Environment, 2022, 829, 154693.	8.0	6
26	Spatial and temporal variations of metal fractions in paddy soil flooding with acid mine drainage. Environmental Research, 2022, 212, 113241.	7.5	8
27	Efficient removal of organophosphate esters by ligand functionalized MIL-101 (Fe): Modulated adsorption and DFT calculations. Chemosphere, 2022, 302, 134881.	8.2	21
28	Twelve natural estrogens in urines of six threatened or endangered mammalian species in Zoo Park: implications and their potential risk. Environmental Science and Pollution Research, 2022, 29, 49404-49410.	5.3	5
29	Influence of protein configuration on aggregation kinetics of nanoplastics in aquatic environment. Water Research, 2022, 219, 118522.	11.3	16
30	Discrepancy strategies of sediment abundant and rare microbial communities in response to floating microplastic disturbances: Study using a microcosmic experiment. Science of the Total Environment, 2022, 835, 155346.	8.0	22
31	Tetracycline-Induced Release and Oxidation of As(III) Coupled with Concomitant Ferrihydrite Transformation. Environmental Science & Technology, 2022, 56, 9453-9462.	10.0	12
32	Memory effect induced the enhancement of uranium (VI) immobilization on low-cost MgAl-double oxide: Mechanism insight and resources recovery. Journal of Hazardous Materials, 2021, 401, 123447.	12.4	49
33	Immobilized Co2+ and Cu2+ induced structural change of layered double hydroxide for efficient heterogeneous degradation of antibiotic. Journal of Hazardous Materials, 2021, 403, 123554.	12.4	20
34	A novel strategy for harmlessness and reduction of copper smelting slags by alkali disaggregation of fayalite (Fe2SiO4) coupling with acid leaching. Journal of Hazardous Materials, 2021, 402, 123791.	12.4	37
35	Making waves: Improving removal performance of conventional wastewater treatment plants on endocrine disrupting compounds (EDCs): their conjugates matter. Water Research, 2021, 188, 116469.	11.3	46
36	Enhanced removal of zinc and cadmium from water using carboxymethyl cellulose-bridged chlorapatite nanoparticles. Chemosphere, 2021, 263, 128038.	8.2	14

#	Article	IF	CITATIONS
37	Differential regulation and the underlying mechanisms of clay minerals to Escherichia coli under the stress of polymyxin B: Comparing halloysite with kaolinite. Chemosphere, 2021, 265, 129095.	8.2	5
38	Mobilization of arsenic during reductive dissolution of As(V)-bearing jarosite by a sulfate reducing bacterium. Journal of Hazardous Materials, 2021, 402, 123717.	12.4	12
39	Simultaneous immobilization of multi-metals in a field contaminated acidic soil using carboxymethyl-cellulose-bridged nano-chlorapatite and calcium oxide. Journal of Hazardous Materials, 2021, 407, 124786.	12.4	18
40	Simultaneous adsorption of Cd2+ and photocatalytic degradation of tris-(2-chloroisopropyl) phosphate (TCPP) by mesoporous TiO2. Chemosphere, 2021, 267, 129238.	8.2	9
41	Photochemical reactivity of nitrogen-doped biochars under simulated sunlight irradiation: Generation of singlet oxygen. Journal of Hazardous Materials, 2021, 410, 124547.	12.4	10
42	Arsenic detoxification by iron-manganese nodules under electrochemically controlled redox: Mechanism and application. Journal of Hazardous Materials, 2021, 403, 123912.	12.4	19
43	Soil rehabilitation shaped different patterns of bacterial and archaeal community in AMD-irrigated paddy soil. Chemosphere, 2021, 263, 128259.	8.2	9
44	Transcriptome profiling of Pseudomonas aeruginosa YH reveals mechanisms of 2, 2′, 4, 4′-tetrabrominated diphenyl ether tolerance and biotransformation. Journal of Hazardous Materials, 2021, 403, 124038.	12.4	18
45	Inhibition of pyrite oxidation using PropS-SH/sepiolite composite coatings for the source control of acid mine drainage. Environmental Science and Pollution Research, 2021, 28, 11090-11105.	5.3	22
46	Sulfate-reducing bacterial community shifts in response to acid mine drainage in the sediment of the Hengshi watershed, South China. Environmental Science and Pollution Research, 2021, 28, 2822-2834.	5.3	20
47	Adsorption of Organic Compounds by Biomass Chars: Direct Role of Aromatic Condensation (Ring) Tj ETQq1 1 (Technology, 2021, 55, 1594-1603.	0.784314 ı 10.0	rgBT /Overloo 16
48	Contribution of nitrogen configurations to the adsorption of Cd(<scp>ii</scp>) in nitrogen-enriched biochar. New Journal of Chemistry, 2021, 45, 12669-12677.	2.8	5
49	Oxygen vacancy-induced donor–acceptor-conjugated microporous poly(triphenylamine–benzothiadiazole)/TiO ₂ as a Z-scheme heterojunction photocatalyst towards a visible-light-driven degradation of bisphenol A. Catalysis Science and Technology, 2021, 11, 1862-1873.	4.1	4
50	Decontamination of dense nonaqueous-phase liquids in groundwater using pump-and-treat and <i>in situ</i> chemical oxidation processes: a field test. RSC Advances, 2021, 11, 4237-4246.	3.6	6
51	Rapid and efficient removal of Cr(<scp>vi</scp>) by a core–shell magnetic mesoporous polydopamine nanocomposite: roles of the mesoporous structure and redox-active functional groups. Journal of Materials Chemistry A, 2021, 9, 13306-13319.	10.3	61
52	Legislation against endocrine-disrupting compounds in drinking water: essential but not enough to ensure water safety. Environmental Science and Pollution Research, 2021, 28, 19505-19510.	5.3	20
53	Inhibition Properties of Arylsulfatase and β-Glucuronidase by Hydrogen Peroxide, Hypochlorite, and Peracetic Acid. ACS Omega, 2021, 6, 8163-8170.	3.5	5
54	Possible overestimation of bisphenol analogues in municipal wastewater analyzed with GC-MS. Environmental Pollution, 2021, 273, 116505.	7.5	18

#	Article	IF	CITATIONS
55	Microbial reduction of As(V)-loaded Schwertmannite by Desulfosporosinus meridiei. Science of the Total Environment, 2021, 764, 144279.	8.0	12
56	Arsenic Partitioning during Schwertmannite Dissolution and Recrystallization in the Presence of Fe(II) and Oxalic Acid. ACS Earth and Space Chemistry, 2021, 5, 1058-1070.	2.7	10
57	Bacterial communities and functional genes stimulated during phenanthrene degradation in soil by bio-microcapsules. Ecotoxicology and Environmental Safety, 2021, 212, 111970.	6.0	21
58	Occurrence and removal of 17α-ethynylestradiol (EE2) in municipal wastewater treatment plants: Current status and challenges. Chemosphere, 2021, 271, 129551.	8.2	49
59	The influence mechanism of dissolved organic matter on the adsorption of Cd (II) by calcite. Environmental Science and Pollution Research, 2021, 28, 37120-37129.	5.3	9
60	Phenanthrene degradation in soil using biochar hybrid modified bio-microcapsules: Determining the mechanism of action via comparative metagenomic analysis. Science of the Total Environment, 2021, 775, 145798.	8.0	17
61	Evaluation of three common alkaline agents for immobilization of multi-metals in a field-contaminated acidic soil. Environmental Science and Pollution Research, 2021, 28, 60765-60777.	5.3	3
62	Removal of heavy metal ions and polybrominated biphenyl ethers by sulfurized nanoscale zerovalent iron: Compound effects and removal mechanism. Journal of Hazardous Materials, 2021, 414, 125555.	12.4	27
63	Far-Less Studied Natural Estrogens as Ignored Emerging Contaminants in Surface Water: Insights from Their Occurrence in the Pearl River, South China. ACS ES&T Water, 2021, 1, 1776-1784.	4.6	11
64	Influence of the co-exposure of microplastics and tetrabromobisphenol A on human gut: Simulation in vitro with human cell Caco-2 and gut microbiota. Science of the Total Environment, 2021, 778, 146264.	8.0	54
65	Mechanisms of Cr(VI) adsorption on schwertmannite under environmental disturbance: Changes in surface complex structures. Journal of Hazardous Materials, 2021, 416, 125781.	12.4	13
66	Self-Activated Ni Cathode for Electrocatalytic Nitrate Reduction to Ammonia: From Fundamentals to Scale-Up for Treatment of Industrial Wastewater. Environmental Science & Technology, 2021, 55, 13231-13243.	10.0	16
67	Effects of ferric ion on the photo-treatment of nonionic surfactant Brij35 washing waste containing 2,2′,4,4′-tetrabromodiphenyl ether. Journal of Hazardous Materials, 2021, 415, 125572.	12.4	9
68	Effects of methanol on the performance of a novel BDE-47 degrading bacterial consortium QY2 in the co-metabolism process. Journal of Hazardous Materials, 2021, 415, 125698.	12.4	21
69	A review of 17α-ethynylestradiol (EE2) in surface water across 32 countries: Sources, concentrations, and potential estrogenic effects. Journal of Environmental Management, 2021, 292, 112804.	7.8	52
70	Sulfate migration and transformation characteristics in paddy soil profile affected by acid mine drainage. Environmental Research, 2021, 200, 111732.	7.5	6
71	Enhanced bioremediation of 2,3′,4,4′,5-pentachlorodiphenyl by consortium GYB1 immobilized on sodium alginate-biochar. Science of the Total Environment, 2021, 788, 147774.	8.0	38
72	Improved extraction of acid-insoluble monosulfide minerals by stannous chloride reduction and its application to the separation of mono- and disulfide minerals in the presence of ferric iron. Science of the Total Environment, 2021, 785, 147367.	8.0	2

#	Article	IF	CITATIONS
73	Enhanced Single and Simultaneous As(III) Adsorption in Pearl River Delta Water by Hexylamine Functionalized Vermiculite. Water (Switzerland), 2021, 13, 2412.	2.7	4
74	Efficient peroxydisulfate activation with nZVI/CuO@BC nanocomposite derived from wastes for degradation of tetrabromobisphenol A in alkaline environment. Journal of Hazardous Materials, 2021, 417, 126029.	12.4	28
75	Co-metabolic and biochar-promoted biodegradation of mixed PAHs by highly efficient microbial consortium QY1. Journal of Environmental Sciences, 2021, 107, 65-76.	6.1	33
76	Bioleaching of indium from waste LCD panels by Aspergillus niger: Method optimization and mechanism analysis. Science of the Total Environment, 2021, 790, 148151.	8.0	21
77	Spatial and temporal variations of Cu and Cd mobility and their controlling factors in pore water of contaminated paddy soil under acid mine drainage: A laboratory column study. Science of the Total Environment, 2021, 792, 148523.	8.0	11
78	Effects of Pyrolysis Temperature and Holding Time on Physicochemical Properties of Swine-Manure-Derived Biochar. Waste and Biomass Valorization, 2020, 11, 613-624.	3.4	37
79	Degradation mechanism, intermediates and toxicology assessment of tris-(2-chloroisopropyl) phosphate using ultraviolet activated hydrogen peroxide. Chemosphere, 2020, 241, 124991.	8.2	14
80	Net heterotrophy and low carbon dioxide emissions from biological processes in the Yellow River Estuary, China. Water Research, 2020, 171, 115457.	11.3	11
81	Synergistic adsorption of Cd(II) and As(V) on birnessite under electrochemical control. Chemosphere, 2020, 247, 125822.	8.2	11
82	Strategy for effective inhibition of arylsulfatase/l²-glucuronidase to prevent deconjugation of sulfate and glucuronide conjugates in wastewater during sample collection and storage. Science of the Total Environment, 2020, 703, 135536.	8.0	17
83	Proteomic mechanism of decabromodiphenyl ether (BDE-209) biodegradation by Microbacterium Y2 and its potential in remediation of BDE-209 contaminated water-sediment system. Journal of Hazardous Materials, 2020, 387, 121708.	12.4	44
84	Human exposure of bisphenol A and its analogues: understandings from human urinary excretion data and wastewater-based epidemiology. Environmental Science and Pollution Research, 2020, 27, 3247-3256.	5.3	49
85	High-efficiency As(III) oxidation and electrocoagulation removal using hematite with a chargeâ^'discharge technique. Science of the Total Environment, 2020, 703, 135678.	8.0	14
86	Global review of phthalates in edible oil: An emerging and nonnegligible exposure source to human. Science of the Total Environment, 2020, 704, 135369.	8.0	56
87	Soil microplastic pollution in an e-waste dismantling zone of China. Waste Management, 2020, 118, 291-301.	7.4	121
88	Remediation of soil and groundwater contaminated with organic chemicals using stabilized nanoparticles: Lessons from the past two decades. Frontiers of Environmental Science and Engineering, 2020, 14, 1.	6.0	28
89	Influence of environmental and biological macromolecules on aggregation kinetics of nanoplastics in aquatic systems. Water Research, 2020, 186, 116316.	11.3	64
90	Oxalate-Induced Photoreduction Dissolution and Transformation of Schwertmannite: Change of Mineral Phase and Elemental Fate. ACS Earth and Space Chemistry, 2020, 4, 2031-2040.	2.7	11

#	Article	IF	CITATIONS
91	Photoassisted degradation of 2,2′,4,4′-tetrabrominated diphenyl ether in simulated soil washing system containing Triton X series surfactants. Environmental Pollution, 2020, 265, 115005.	7.5	7
92	Effects of adsorbed phosphate on jarosite reduction by a sulfate reducing bacterium and associated mineralogical transformation. Ecotoxicology and Environmental Safety, 2020, 202, 110921.	6.0	3
93	Leaching characteristics of heavy metals in tailings and their simultaneous immobilization with triethylenetetramine functioned montmorillonite (TETA-Mt) against simulated acid rain. Environmental Pollution, 2020, 266, 115236.	7.5	42
94	Debromination of polybrominated diphenyl ethers (PBDEs) by palladized zerovalent zinc particles: Influence factors, pathways and mechanism. Chemosphere, 2020, 253, 126726.	8.2	6
95	Arsenic behavior during gallic acid-induced redox transformation of jarosite under acidic conditions. Chemosphere, 2020, 255, 126938.	8.2	18
96	Viability and distribution of bacteria immobilized on Sawdust@silica: The removal mechanism of phenanthrene in soil. Ecotoxicology and Environmental Safety, 2020, 198, 110649.	6.0	4
97	Acidity and metallic elements release from AMD-affected river sediments: Effect of AMD standstill and dilution. Environmental Research, 2020, 186, 109490.	7.5	26
98	Remediation of heavy metal contaminated soils by organic acid extraction and electrochemical adsorption. Environmental Pollution, 2020, 264, 114745.	7.5	85
99	Trace determination of eleven natural estrogens and insights from their occurrence in a municipal wastewater treatment plant and river water. Water Research, 2020, 182, 115976.	11.3	40
100	Adhesion of Sphingomonas sp. GY2B onto montmorillonite: A combination study by thermodynamics and the extended DLVO theory. Colloids and Surfaces B: Biointerfaces, 2020, 192, 111085.	5.0	21
101	Effect of nitrate on the phototreatment of Triton X-100 simulated washing waste containing 4,4′-dibromodiphenyl ether: Kinetics, products and toxicity assessment. Science of the Total Environment, 2020, 732, 139247.	8.0	16
102	Transcriptome Analysis of the Acid Stress Response of Desulfovibrio vulgaris ATCC 7757. Current Microbiology, 2020, 77, 2702-2712.	2.2	7
103	The formation pathways of polybrominated dibenzo-p-dioxins and dibenzofurans (PBDD/Fs) from pyrolysis of polybrominated diphenyl ethers (PBDEs): Effects of bromination arrangement and level. Journal of Hazardous Materials, 2020, 399, 123004.	12.4	12
104	Co-metabolic degradation of tetrabromobisphenol A by Pseudomonas aeruginosa and its auto-poisoning effect caused during degradation process. Ecotoxicology and Environmental Safety, 2020, 202, 110919.	6.0	9
105	Cellular changes of microbial consortium GY1 during decabromodiphenyl ether (BDE-209) biodegradation and identification of strains responsible for BDE-209 degradation in GY1. Chemosphere, 2020, 249, 126205.	8.2	19
106	Fate of oxalic-acid-intervened arsenic during Fe(II)-induced transformation of As(V)-bearing jarosite. Science of the Total Environment, 2020, 719, 137311.	8.0	18
107	Multifunctional magnetic MgMn-oxide composite for efficient purification of Cd2+ and paracetamol pollution: Synergetic effect and stability. Journal of Hazardous Materials, 2020, 388, 122078.	12.4	41
108	Bisphenol analogues in Chinese bottled water: Quantification and potential risk analysis. Science of the Total Environment, 2020, 713, 136583.	8.0	88

#	Article	IF	CITATIONS
109	Promoting the photogeneration of hydrochar reactive oxygen species based on FeAl layered double hydroxide for diethyl phthalate degradation. Journal of Hazardous Materials, 2020, 388, 122120.	12.4	32
110	Removal of triphenyl phosphate by nanoscale zerovalent iron (nZVI) activated bisulfite: Performance, surface reaction mechanism and sulfate radical-mediated degradation pathway. Environmental Pollution, 2020, 260, 113983.	7.5	34
111	Biodegradation of triphenyl phosphate using an efficient bacterial consortium GYY: Degradation characteristics, metabolic pathway and 16S rRNA genes analysis. Science of the Total Environment, 2020, 713, 136598.	8.0	24
112	Incorporation of Pb(<scp>ii</scp>) into hematite during ferrihydrite transformation. Environmental Science: Nano, 2020, 7, 829-841.	4.3	16
113	Electrochemical adsorption of cadmium and arsenic by natural Fe-Mn nodules. Journal of Hazardous Materials, 2020, 390, 122165.	12.4	26
114	Efficient degradation of sodium diclofenac via heterogeneous Fenton reaction boosted by Pd/Fe@Fe3O4 nanoparticles derived from bio-recovered palladium. Journal of Environmental Management, 2020, 260, 110072.	7.8	34
115	Bacterial communities on soil microplastic at Guiyu, an E-Waste dismantling zone of China. Ecotoxicology and Environmental Safety, 2020, 195, 110521.	6.0	62
116	Removal of hexavalent chromium using biogenic mackinawite (FeS)-deposited kaolinite. Journal of Colloid and Interface Science, 2020, 572, 236-245.	9.4	39
117	Degradation of trichloroethylene by photoelectrochemically activated persulfate. Chemosphere, 2020, 254, 126796.	8.2	16
118	Chemodiversity of Soil Dissolved Organic Matter. Environmental Science & Technology, 2020, 54, 6174-6184.	10.0	133
119	Reductive debromination of decabromodiphenyl ether by iron sulfide-coated nanoscale zerovalent iron: mechanistic insights from Fe(II) dissolution and solvent kinetic isotope effects. Environmental Pollution, 2019, 253, 161-170.	7.5	37
120	Aggregation kinetics of UV irradiated nanoplastics in aquatic environments. Water Research, 2019, 163, 114870.	11.3	116
121	Reductive dissolution of jarosite by a sulfate reducing bacterial community: Secondary mineralization and microflora development. Science of the Total Environment, 2019, 690, 1100-1109.	8.0	37
122	Insights into removal mechanisms of bisphenol A and its analogues in municipal wastewater treatment plants. Science of the Total Environment, 2019, 692, 107-116.	8.0	116
123	OPFRs and BFRs induced A549â€ ⁻ cell apoptosis by caspase-dependent mitochondrial pathway. Chemosphere, 2019, 221, 693-702.	8.2	60
124	Mechanisms and pathways of debromination of polybrominated diphenyl ethers (PBDEs) in various nano-zerovalent iron-based bimetallic systems. Science of the Total Environment, 2019, 661, 18-26.	8.0	42
125	Ferrihydrite transformation under the impact of humic acid and Pb: kinetics, nanoscale mechanisms, and implications for C and Pb dynamics. Environmental Science: Nano, 2019, 6, 747-762.	4.3	59
126	The behavior of chromium and arsenic associated with redox transformation of schwertmannite in AMD environment. Chemosphere, 2019, 222, 945-953.	8.2	54

#	Article	IF	CITATIONS
127	Modeling Sorptive Fractionation of Organic Matter at the Mineralâ€Water Interface. Soil Science Society of America Journal, 2019, 83, 107-117.	2.2	9
128	Effects of benzo [a] pyrene (BaP) on the composting and microbial community of sewage sludge. Chemosphere, 2019, 222, 517-526.	8.2	30
129	Biodegradation of tricresyl phosphate isomers by Brevibacillus brevis: Degradation pathway and metabolic mechanism. Chemosphere, 2019, 232, 195-203.	8.2	24
130	Coupled Kinetics Model for Microbially Mediated Arsenic Reduction and Adsorption/Desorption on Iron Oxides: Role of Arsenic Desorption Induced by Microbes. Environmental Science & Technology, 2019, 53, 8892-8902.	10.0	30
131	Mechanism of enhancing pyrene-degradation ability of bacteria by layer-by-layer assembly bio-microcapsules materials. Ecotoxicology and Environmental Safety, 2019, 181, 525-533.	6.0	7
132	Oxidation degradation of tris-(2-chloroisopropyl) phosphate by ultraviolet driven sulfate radical: Mechanisms and toxicology assessment of degradation intermediates using flow cytometry analyses. Science of the Total Environment, 2019, 687, 732-740.	8.0	26
133	A simulation-based bi-level multi-objective programming model for watershed water quality management under interval and stochastic uncertainties. Journal of Environmental Management, 2019, 245, 418-431.	7.8	12
134	Environmental application of MgMn-layered double oxide for simultaneous efficient removal of tetracycline and Cd pollution: Performance and mechanism. Journal of Environmental Management, 2019, 246, 164-173.	7.8	64
135	Biogenic iron mineralization of polyferric sulfate by dissimilatory iron reducing bacteria: Effects of medium composition and electric field stimulation. Science of the Total Environment, 2019, 684, 466-475.	8.0	14
136	Molecular fractionation and sub-nanoscale distribution of dissolved organic matter on allophane. Environmental Science: Nano, 2019, 6, 2037-2048.	4.3	26
137	Ag/AgCl/MIL-101(Fe) Catalyzed Degradation of Methylene Blue under Visible Light Irradation. Materials, 2019, 12, 1453.	2.9	20
138	Predicting Kinetics of As(V) Adsorption and Desorption on Mixed Minerals of Ferrihydrite and δâ€MnO ₂ . Soil Science Society of America Journal, 2019, 83, 348-356.	2.2	4
139	Effective capture of aqueous uranium from saline lake with magnesium-based binary and ternary layered double hydroxides. Science of the Total Environment, 2019, 677, 556-563.	8.0	51
140	Degradation of tris(2-chloroethyl) phosphate (TCEP) in aqueous solution by using pyrite activating persulfate to produce radicals. Ecotoxicology and Environmental Safety, 2019, 174, 667-674.	6.0	62
141	Synergistic deep removal of As(III) and Cd(II) by a calcined multifunctional MgZnFe-CO3 layered double hydroxide: Photooxidation, precipitation and adsorption. Chemosphere, 2019, 225, 115-125.	8.2	64
142	Core-shell structured Fe3O4@GO@MIL-100(Fe) magnetic nanoparticles as heterogeneous photo-Fenton catalyst for 2,4-dichlorophenol degradation under visible light. Journal of Hazardous Materials, 2019, 371, 677-686.	12.4	121
143	High mineral adsorption of glyphosate versus diethyl phthalate and tetracycline, during visible light photodegradation with goethite and oxalate. Environmental Chemistry Letters, 2019, 17, 1421-1428.	16.2	13
144	The effects of interaction between vermiculite and manganese dioxide on the environmental geochemical process of thallium. Science of the Total Environment, 2019, 669, 903-910.	8.0	32

#	Article	IF	CITATIONS
145	Bioaccumulation and distribution of cadmium by Burkholderia cepacia GYP1 under oligotrophic condition and mechanism analysis at proteome level. Ecotoxicology and Environmental Safety, 2019, 176, 162-169.	6.0	44
146	Dissimilatory iron and sulfate reduction by native microbial communities using lactate and citrate as carbon sources and electron donors. Ecotoxicology and Environmental Safety, 2019, 174, 524-531.	6.0	48
147	Sustainable Water Resource Management of Regulated Rivers under Uncertain Inflow Conditions Using a Noisy Genetic Algorithm. International Journal of Environmental Research and Public Health, 2019, 16, 868.	2.6	5
148	Biodegradation of decabromodiphenyl ether (BDE-209) using a novel microbial consortium GY1: Cells viability, pathway, toxicity assessment, and microbial function prediction. Science of the Total Environment, 2019, 668, 958-965.	8.0	46
149	Degradation of 2,2′,4,4′-tetrabromodiphenyl ether by Pycnoporus sanguineus in the presence of copper ions. Journal of Environmental Sciences, 2019, 83, 133-143.	6.1	6
150	Photocatalytic debromination of polybrominated diphenyl ethers (PBDEs) on metal doped TiO2 nanocomposites: Mechanisms and pathways. Environment International, 2019, 127, 5-12.	10.0	49
151	Insights into the Glyphosate Adsorption Behavior and Mechanism by a MnFe ₂ O ₄ @Cellulose-Activated Carbon Magnetic Hybrid. ACS Applied Materials & Interfaces, 2019, 11, 15478-15488.	8.0	83
152	Pyrene Degradation by Mycobacterium gilvum: Metabolites and Proteins Involved. Water, Air, and Soil Pollution, 2019, 230, 1.	2.4	15
153	Photocatalytic degradation of polybrominated biphenyls (PBBs) on metal doped TiO ₂ nanocomposites in aqueous environments: mechanisms and solution effects. Environmental Science: Nano, 2019, 6, 1111-1120.	4.3	8
154	Bioremediation of triphenyl phosphate in river water microcosms: Proteome alteration of Brevibacillus brevis and cytotoxicity assessments. Science of the Total Environment, 2019, 649, 563-570.	8.0	21
155	Thiocyanate-induced labilization of schwertmannite: Impacts and mechanisms. Journal of Environmental Sciences, 2019, 80, 218-228.	6.1	20
156	Rate constants for the reaction of hydroxyl and sulfate radicals with organophosphorus esters (OPEs) determined by competition method. Ecotoxicology and Environmental Safety, 2019, 170, 300-305.	6.0	17
157	Trace determination of sulfonamide antibiotics and their acetylated metabolites via SPE-LC-MS/MS in wastewater and insights from their occurrence in a municipal wastewater treatment plant. Science of the Total Environment, 2019, 653, 815-821.	8.0	99
158	Transformation of cadmium-associated schwertmannite and subsequent element repartitioning behaviors. Environmental Science and Pollution Research, 2019, 26, 617-627.	5.3	19
159	Effects of surfactant on the degradation of 2,2′,4,4′-tetrabromodiphenyl ether (BDE-47) by nanoscale Ag/Fe particles: Kinetics, mechanisms and intermediates. Environmental Pollution, 2019, 245, 780-788.	7.5	16
160	Effect of phosphate on amorphous iron mineral generation and arsenic behavior in paddy soils. Science of the Total Environment, 2019, 657, 644-656.	8.0	35
161	Identification of novel pathways for biotransformation of tetrabromobisphenol A by Phanerochaete chrysosporium, combined with mechanism analysis at proteome level. Science of the Total Environment, 2019, 659, 1352-1361.	8.0	39
162	Performance evaluation of integrated adsorption-nanofiltration system for emerging compounds removal: Exemplified by caffeine, diclofenac and octylphenol. Journal of Environmental Management, 2019, 231, 121-128.	7.8	39

#	Article	IF	CITATIONS
163	Cd2+ adsorption performance of tunnel-structured manganese oxides driven by electrochemically controlled redox. Environmental Pollution, 2019, 244, 783-791.	7.5	33
164	Molecular characteristics, proton dissociation properties, and metal binding properties of soil organic matter: A theoretical study. Science of the Total Environment, 2019, 656, 521-530.	8.0	29
165	Bisphenol A concentrations in human urine, human intakes across six continents, and annual trends of average intakes in adult and child populations worldwide: A thorough literature review. Science of the Total Environment, 2018, 626, 971-981.	8.0	133
166	Sulfate-reducing bacteria in anaerobic bioprocesses: basic properties of pure isolates, molecular quantification, and controlling strategies. Environmental Technology Reviews, 2018, 7, 46-72.	4.3	24
167	Effects of eggshell addition on calcium-deficient acid soils contaminated with heavy metals. Frontiers of Environmental Science and Engineering, 2018, 12, 1.	6.0	8
168	Maize straw decorated with sulfide for tylosin removal from the water. Ecotoxicology and Environmental Safety, 2018, 152, 16-23.	6.0	43
169	Characterization of a di-n-butyl phthalate-degrading bacterial consortium and its application in contaminated soil. Environmental Science and Pollution Research, 2018, 25, 17645-17653.	5.3	32
170	Enhanced photoelectrochemical degradation of Ibuprofen and generation of hydrogen via BiOI-deposited TiO2 nanotube arrays. Science of the Total Environment, 2018, 633, 1198-1205.	8.0	27
171	Simultaneous electricity production and antibiotics removal by microbial fuel cells. Journal of Environmental Management, 2018, 217, 565-572.	7.8	71
172	Debromination of polybrominated diphenyl ethers (PBDEs) by zero valent zinc: Mechanisms and predicting descriptors. Journal of Hazardous Materials, 2018, 352, 165-171.	12.4	28
173	Effect of Cu(II) on the stability of oxyanion-substituted schwertmannite. Environmental Science and Pollution Research, 2018, 25, 15492-15506.	5.3	9
174	Sorption of crude oil by enzyme-modified corn stalk vs. chemically treated corn stalk. Journal of Molecular Liquids, 2018, 255, 324-332.	4.9	17
175	Differential regulation of phenanthrene biodegradation process by kaolinite and quartz and the underlying mechanism. Journal of Hazardous Materials, 2018, 349, 51-59.	12.4	37
176	Enhanced Adsorption of <i>p</i> -Arsanilic Acid from Water by Amine-Modified UiO-67 as Examined Using Extended X-ray Absorption Fine Structure, X-ray Photoelectron Spectroscopy, and Density Functional Theory Calculations. Environmental Science & Technology, 2018, 52, 3466-3475.	10.0	148
177	Complexation of sulfamethazine with Cd(II) and Pb(II): implication for co-adsorption of SMT and Cd(II) on goethite. Environmental Science and Pollution Research, 2018, 25, 11576-11583.	5.3	24
178	Defective magnesium ferrite nano-platelets for the adsorption of As(V): The role of surface hydroxyl groups. Environmental Pollution, 2018, 235, 11-19.	7.5	46
179	Debromination of polybrominated diphenyl ethers (PBDEs) and their conversion to polybrominated dibenzofurans (PBDFs) by UV light: Mechanisms and pathways. Journal of Hazardous Materials, 2018, 354, 1-7.	12.4	39
180	Photocatalytic removal of organic phosphate esters by TiO2: Effect of inorganic ions and humic acid. Chemosphere, 2018, 206, 26-32.	8.2	75

#	Article	IF	CITATIONS
181	Bioremediation of triphenyl phosphate by Brevibacillus brevis: Degradation characteristics and role of cytochrome P450 monooxygenase. Science of the Total Environment, 2018, 627, 1389-1395.	8.0	57
182	Time-dependent bacterial community and electrochemical characterizations of cathodic biofilms in the surfactant-amended sediment-based bioelectrochemical reactor with enhanced 2,3,4,5-tetrachlorobiphenyl dechlorination. Environmental Pollution, 2018, 236, 343-354.	7.5	16
183	Role of microbial activity in Fe(III) hydroxysulfate mineral transformations in an acid mine drainage-impacted site from the Dabaoshan Mine. Science of the Total Environment, 2018, 616-617, 647-657.	8.0	80
184	Bioremediation of PAH-contaminated farmland: field experiment. Environmental Science and Pollution Research, 2018, 25, 64-72.	5.3	14
185	Photodegradation behaviors of polychlorinated biphenyls in methanol by UV-irradiation: Solvent adducts and sigmatropic arrangement. Chemosphere, 2018, 193, 861-868.	8.2	15
186	Effect of 2, 2′, 4, 4′-tetrabromodiphenyl ether (BDE-47) and its metabolites on cell viability, oxidative stress, and apoptosis of HepG2. Chemosphere, 2018, 193, 978-988.	8.2	54
187	Fast trace determination of nine odorant and estrogenic chloro- and bromo-phenolic compounds in real water samples through automated solid-phase extraction coupled with liquid chromatography tandem mass spectrometry. Environmental Science and Pollution Research, 2018, 25, 3813-3822.	5.3	34
188	A novel multi-reaction model for kinetics of Zn release from soils: Roles of soil binding sites. Journal of Colloid and Interface Science, 2018, 514, 146-155.	9.4	22
189	Bacterial, archaeal, and fungal community responses to acid mine drainage-laden pollution in a rice paddy soil ecosystem. Science of the Total Environment, 2018, 616-617, 107-116.	8.0	93
190	Migration and potential risk of trace phthalates in bottled water: AÂglobal situation. Water Research, 2018, 147, 362-372.	11.3	134
191	Effective Extraction of Cr(VI) from Hazardous Gypsum Sludge via Controlling the Phase Transformation and Chromium Species. Environmental Science & Technology, 2018, 52, 13336-13342.	10.0	175
192	Coupled Kinetics of Ferrihydrite Transformation and As(V) Sequestration under the Effect of Humic Acids: A Mechanistic and Quantitative Study. Environmental Science & Technology, 2018, 52, 11632-11641.	10.0	34
193	Debromination of 2,2′,4,4′-tetrabromodiphenyl ether (BDE-47) by synthetic Pd/FeO and Cu/FeO in different protic solvents. Chemosphere, 2018, 212, 946-953.	8.2	12
194	Rapid debromination of polybrominated diphenyl ethers (PBDEs) by zero valent metal and bimetals: Mechanisms and pathways assisted by density function theory calculation. Environmental Pollution, 2018, 240, 745-753.	7.5	29
195	Microbial Reduction of Cr (VI)-loaded Schwertmannite by <i>Shewanella oneidensis</i> MR-1. Geomicrobiology Journal, 2018, 35, 727-734.	2.0	15
196	iTRAQ-based proteomic profiling of Pycnoporus sanguineus in response to co-existed tetrabromobisphenol A (TBBPA) and hexavalent chromium. Environmental Pollution, 2018, 242, 1758-1767.	7.5	22
197	Schwertmannite transformation via direct or indirect electron transfer by a sulfate reducing enrichment culture. Environmental Pollution, 2018, 242, 738-748.	7.5	20
198	Immobilization of Sphingomonas sp. GY2B in polyvinyl alcohol–alginate–kaolin beads for efficient degradation of phenol against unfavorable environmental factors. Ecotoxicology and Environmental Safety, 2018, 162, 103-111.	6.0	88

#	Article	IF	CITATIONS
199	Cadmium-induced stress response of Phanerochaete chrysosporium during the biodegradation of 2,2′,4,4′-tetrabromodiphenyl ether (BDE-47). Ecotoxicology and Environmental Safety, 2018, 154, 45-51.	6.0	15
200	Biomineralization mechanism of U(VI) induced by Bacillus cereus 12-2: The role of functional groups and enzymes. Chemosphere, 2018, 206, 682-692.	8.2	43
201	Experimental and theoretical investigations on debromination pathways of polybrominated biphenyls (PBBs) under ultraviolet light. Chemosphere, 2018, 212, 1-7.	8.2	4
202	Migration and fate of metallic elements in a waste mud impoundment and affected river downstream: A case study in Dabaoshan Mine, South China. Ecotoxicology and Environmental Safety, 2018, 164, 474-483.	6.0	37
203	Mineralogical characteristics of sediments and heavy metal mobilization along a river watershed affected by acid mine drainage. PLoS ONE, 2018, 13, e0190010.	2.5	48
204	Relative roles of H-atom transfer and electron transfer in the debromination of polybrominated diphenyl ethers by palladized nanoscale zerovalent iron. Environmental Pollution, 2017, 222, 331-337.	7.5	41
205	Refocusing on Nonpriority Toxic Metals in the Aquatic Environment in China. Environmental Science & Technology, 2017, 51, 3117-3118.	10.0	55
206	Distribution, fractionation, and contamination assessment of heavy metals in paddy soil related to acid mine drainage. Paddy and Water Environment, 2017, 15, 553-562.	1.8	25
207	Photodebromination behaviors of polybrominated diphenyl ethers in methanol/water systems: Mechanisms and predicting descriptors. Science of the Total Environment, 2017, 595, 666-672.	8.0	17
208	Photodegradation of 4,4′-dibrominated diphenyl ether in Triton X-100 micellar solution. Chemosphere, 2017, 180, 423-429.	8.2	23
209	Influence of co-existed tetrabromobisphenol A (TBBPA) and hexavalent chromium on the cellular characteristics of Pycnoporus sanguineus during their removal and reduction. Ecotoxicology and Environmental Safety, 2017, 142, 388-398.	6.0	18
210	Effects of single and combined copper/perfluorooctane sulfonate on sequencing batch reactor process and microbial community in activated sludge. Bioresource Technology, 2017, 238, 407-415.	9.6	37
211	Removal of heavy metals from acid mine drainage using chicken eggshells in column mode. Journal of Environmental Management, 2017, 188, 1-8.	7.8	44
212	Hexavalent chromium induced oxidative stress and apoptosis in Pycnoporus sanguineus. Environmental Pollution, 2017, 228, 128-139.	7.5	67
213	Biosurfactant rhamnolipid enhanced modification of corn stalk and its application for sorption of phenanthrene. Water Science and Technology, 2017, 76, 1167-1176.	2.5	0
214	Worldwide human daily intakes of bisphenol A (BPA) estimated from global urinary concentration data (2000–2016) and its risk analysis. Environmental Pollution, 2017, 230, 143-152.	7.5	151
215	The double influence mechanism of pH on arsenic removal by nano zero valent iron: electrostatic interactions and the corrosion of Fe ⁰ . Environmental Science: Nano, 2017, 4, 1544-1552.	4.3	78
216	Effects of rhamnolipids on the cell surface characteristics of Sphingomonas sp. GY2B and the biodegradation of phenanthrene. RSC Advances, 2017, 7, 24321-24330.	3.6	25

#	Article	IF	CITATIONS
217	Amphoteric modified vermiculites as adsorbents for enhancing removal of organic pollutants: Bisphenol A and Tetrabromobisphenol A. Environmental Pollution, 2017, 228, 277-286.	7.5	79
218	Drivers and applications of integrated clean-up technologies for surfactant-enhanced remediation of environments contaminated with polycyclic aromatic hydrocarbons (PAHs). Environmental Pollution, 2017, 225, 129-140.	7.5	95
219	Predicting criteria continuous concentrations of metals or metalloids for protecting marine life by use of quantitative ion characteristic–activity relationships–species sensitivity distributions (QICAR-SSD). Marine Pollution Bulletin, 2017, 124, 639-644.	5.0	14
220	Biodegradation of 2,2′,4,4′-tetrabromodiphenyl ether (BDE-47) by Phanerochaete chrysosporium in the presence of Cd2+. Environmental Science and Pollution Research, 2017, 24, 11415-11424.	5.3	23
221	Characteristics and proteomic analysis of pyrene degradation by Brevibacillus brevis in liquid medium. Chemosphere, 2017, 178, 80-87.	8.2	37
222	Pyrene biodegradation with layer-by-layer assembly bio-microcapsules. Ecotoxicology and Environmental Safety, 2017, 138, 9-15.	6.0	18
223	Comparative proteomics reveal the mechanism of Tween80 enhanced phenanthrene biodegradation by Sphingomonas sp. GY2B. Ecotoxicology and Environmental Safety, 2017, 137, 256-264.	6.0	36
224	Layer-by-layer assembly surface modified microbial biomass for enhancing biorecovery of secondary gold. Waste Management, 2017, 60, 552-560.	7.4	11
225	CoMn2O4-supported functionalized carbon nanotube: efficient catalyst for oxygen reduction in microbial fuel cells. Journal of Nanoparticle Research, 2017, 19, 1.	1.9	5
226	Biogenic Calcium Carbonate with Hierarchical Organic–Inorganic Composite Structure Enhancing the Removal of Pb(II) from Wastewater. ACS Applied Materials & Interfaces, 2017, 9, 35785-35793.	8.0	67
227	Effects of Cd(II) on the stability of humic acid-coated nano-TiO2 particles in aquatic environments. Environmental Science and Pollution Research, 2017, 24, 23144-23152.	5.3	6
228	Enhanced removal of roxarsone by Fe ₃ O ₄ @3D graphene nanocomposites: synergistic adsorption and mechanism. Environmental Science: Nano, 2017, 4, 2134-2143.	4.3	89
229	Isotope geochemistry, hydrochemistry, and mineralogy of a river affected by acid mine drainage in a mining area, South China. RSC Advances, 2017, 7, 43310-43318.	3.6	20
230	Effects of modified biochar on rhizosphere microecology of rice (Oryza sativa L.) grown in As-contaminated soil. Environmental Science and Pollution Research, 2017, 24, 23815-23824.	5.3	35
231	Mechanisms of Synergistic Removal of Low Concentration As(V) by nZVI@Mg(OH) ₂ Nanocomposite. Journal of Physical Chemistry C, 2017, 121, 21411-21419.	3.1	18
232	Comparative transcriptomic evidence for Tween80-enhanced biodegradation of phenanthrene by Sphingomonas sp. GY2B. Science of the Total Environment, 2017, 609, 1161-1171.	8.0	36
233	Simultaneous determination of eleven estrogenic and odorous chloro- and bromo-phenolic compounds in surface water through an automated online headspace SPME followed by on-fiber derivatization coupled with GC-MS. Analytical Methods, 2017, 9, 4819-4827.	2.7	31
234	Kinetics of Cation and Oxyanion Adsorption and Desorption on Ferrihydrite: Roles of Ferrihydrite Binding Sites and a Unified Model. Environmental Science & Technology, 2017, 51, 10605-10614.	10.0	115

#	Article	lF	CITATIONS
235	Biomass-derived heteroatoms-doped mesoporous carbon for efficient oxygen reduction in microbial fuel cells. Biosensors and Bioelectronics, 2017, 98, 350-356.	10.1	92
236	Do estrogenic compounds in drinking water migrating from plastic pipe distribution system pose adverse effects to human? An analysis of scientific literature. Environmental Science and Pollution Research, 2017, 24, 2126-2134.	5.3	32
237	Fe- and S-Metabolizing Microbial Communities Dominate an AMD-Contaminated River Ecosystem and Play Important Roles in Fe and S Cycling. Geomicrobiology Journal, 2017, 34, 695-705.	2.0	24
238	Evaluation of the physiochemical properties and catalytic performance of mixed metal oxides-carbon nanotubes nanohybrids containing carbon nanotubes with different diameters. Applied Clay Science, 2017, 135, 95-102.	5.2	7
239	Heavy Metal Contamination and Health Risk Assessment in the Vicinity of a Tailing Pond in Guangdong, China. International Journal of Environmental Research and Public Health, 2017, 14, 1557.	2.6	138
240	Role of Dissolved Organic Matter in the Release of Chromium from Schwertmannite: Kinetics, Repartition, and Mechanisms. Journal of Environmental Quality, 2017, 46, 1088-1097.	2.0	16
241	Effects of cytotoxicity of erythromycin on PAH-degrading strains and degrading efficiency. RSC Advances, 2016, 6, 114396-114404.	3.6	4
242	Levels of six antibiotics used in China estimated by means of wastewater-based epidemiology. Water Science and Technology, 2016, 73, 769-775.	2.5	31
243	Fate of Fe and Cd upon microbial reduction of Cd-loaded polyferric flocs by Shewanella oneidensis MR-1. Chemosphere, 2016, 144, 2065-2072.	8.2	60
244	Nonionic surfactants induced changes in cell characteristics and phenanthrene degradation ability of Sphingomonas sp. GY2B. Ecotoxicology and Environmental Safety, 2016, 129, 210-218.	6.0	72
245	Atomistic Simulation of Solubilization of Polycyclic Aromatic Hydrocarbons in a Sodium Dodecyl Sulfate Micelle. Langmuir, 2016, 32, 3645-3654.	3.5	16
246	A new approach for pyrene bioremediation using bacteria immobilized in layer-by-layer assembled microcapsules: dynamics of soil bacterial community. RSC Advances, 2016, 6, 20654-20663.	3.6	26
247	Synergetic effect of functionalized carbon nanotubes on ZnCr–mixed metal oxides for enhanced solar light-driven photocatalytic performance. RSC Advances, 2016, 6, 37689-37700.	3.6	21
248	Kinetics of Heavy Metal Dissociation from Natural Organic Matter: Roles of the Carboxylic and Phenolic Sites. Environmental Science & amp; Technology, 2016, 50, 10476-10484.	10.0	91
249	Efficient inhibition of heavy metal release from mine tailings against acid rain exposure by triethylenetetramine intercalated montmorillonite (TETA-Mt). Journal of Hazardous Materials, 2016, 318, 396-406.	12.4	43
250	Bioremediation of Petroleum-Contaminated Acid Soil by a Constructed Bacterial Consortium Immobilized on Sawdust: Influences of Multiple Factors. Water, Air, and Soil Pollution, 2016, 227, 1.	2.4	16
251	Simultaneous determination of estrogenic odorant alkylphenols, chlorophenols, and their derivatives in water using online headspace solid phase microextraction coupled with gas chromatography-mass spectrometry. Environmental Science and Pollution Research, 2016, 23, 19116-19125.	5.3	31
252	Mn ₂ O ₃ hollow spheres synthesized based on an ion-exchange strategy from amorphous calcium carbonate for highly efficient trace-level uranyl extraction. Environmental Science: Nano, 2016, 3, 1254-1258.	4.3	32

#	Article	IF	CITATIONS
253	A bio-hybrid material for adsorption and degradation of phenanthrene: bacteria immobilized on sawdust coated with a silica layer. RSC Advances, 2016, 6, 107189-107199.	3.6	10
254	Sorption of tylosin and sulfamethazine on solid humic acid. Journal of Environmental Sciences, 2016, 43, 208-215.	6.1	34
255	Effects of nano bamboo charcoal on PAHs-degrading strain Sphingomonas sp. GY2B. Ecotoxicology and Environmental Safety, 2016, 125, 35-42.	6.0	28
256	Physiological responses of Microcystis aeruginosa against the algicidal bacterium Pseudomonas aeruginosa. Ecotoxicology and Environmental Safety, 2016, 127, 214-221.	6.0	51
257	Enhanced degradation of phenol by Sphingomonas sp. GY2B with resistance towards suboptimal environment through adsorption on kaolinite. Chemosphere, 2016, 148, 388-394.	8.2	42
258	Simultaneous Cr(VI) removal and 2,2′,4,4′-tetrabromodiphenyl ether (BDE-47) biodegradation by Pseudomonas aeruginosa in liquid medium. Chemosphere, 2016, 150, 24-32.	8.2	34
259	Aerobic degradation of BDE-209 by Enterococcus casseliflavus: Isolation, identification and cell changes during degradation process. Journal of Hazardous Materials, 2016, 308, 335-342.	12.4	59
260	Metabolic biotransformation of copper–benzo[a]pyrene combined pollutant on the cellular interface of Stenotrophomonas maltophilia. Bioresource Technology, 2016, 204, 26-31.	9.6	17
261	Electrokinetic-Enhanced Remediation of Phenanthrene-Contaminated Soil Combined with Sphingomonas sp. GY2B and Biosurfactant. Applied Biochemistry and Biotechnology, 2016, 178, 1325-1338.	2.9	12
262	Preparation and characterization of ZnTiO3–TiO2/pillared montmorillonite composite catalyst for enhanced photocatalytic activity. Research on Chemical Intermediates, 2016, 42, 5253-5268.	2.7	12
263	Ecotoxicity monitoring and bioindicator screening of oil-contaminated soil during bioremediation. Ecotoxicology and Environmental Safety, 2016, 124, 120-128.	6.0	55
264	Cosolubilization synergism occurrence in codesorption of PAH mixtures during surfactant-enhanced remediation of contaminated soil. Chemosphere, 2016, 144, 583-590.	8.2	22
265	Removal of Natural Estrogens and Their Conjugates in Municipal Wastewater Treatment Plants: A Critical Review. Environmental Science & Technology, 2015, 49, 5288-5300.	10.0	137
266	Nickel oxide and carbon nanotube composite (NiO/CNT) as a novel cathode non-precious metal catalyst in microbial fuel cells. Biosensors and Bioelectronics, 2015, 72, 332-339.	10.1	162
267	Sorption and photodegradation of tylosin and sulfamethazine by humic acid-coated goethite. RSC Advances, 2015, 5, 100464-100471.	3.6	23
268	Effect of Pb ²⁺ , Cd ²⁺ , Cu ²⁺ and dissolved organic carbon (DOC) on the distribution and partition of decabromodiphenyl ether (BDE-209) in a water–sediment system. RSC Advances, 2015, 5, 105259-105265.	3.6	0
269	Biosorption and biodegradation of pyrene by Brevibacillus brevis and cellular responses to pyrene treatment. Ecotoxicology and Environmental Safety, 2015, 115, 166-173.	6.0	37
270	Effects of humic acids on the aggregation and sorption of nano-TiO2. Chemosphere, 2015, 119, 171-176.	8.2	40

#	Article	IF	CITATIONS
271	Sorption behavior of tylosin and sulfamethazine on humic acid: kinetic and thermodynamic studies. RSC Advances, 2015, 5, 58865-58872.	3.6	57
272	Understanding the role of clay minerals in the chromium(VI) bioremoval by Pseudomonas aeruginosa CCTCC AB93066 under growth condition: microscopic, spectroscopic and kinetic analysis. World Journal of Microbiology and Biotechnology, 2015, 31, 1765-1779.	3.6	21
273	Effect of surfactant amendment to PAHs-contaminated soil for phytoremediation by maize (Zea mays) Tj ETQq1 1	0.784314 6.0	1 rgBT /Over
274	Sulfate migration in a river affected by acid mine drainage from the Dabaoshan mining area, South China. Chemosphere, 2015, 119, 734-743.	8.2	83
275	Bioaccumulation characterization of cadmium by growing Bacillus cereus RC-1 and its mechanism. Chemosphere, 2014, 109, 134-142.	8.2	109
276	Influence of co-existed benzo[a]pyrene and copper on the cellular characteristics of Stenotrophomonas maltophilia during biodegradation and transformation. Bioresource Technology, 2014, 158, 181-187.	9.6	64
277	Tea saponin enhanced biodegradation of decabromodiphenyl ether by Brevibacillus brevis. Chemosphere, 2014, 114, 255-261.	8.2	26
	Estimation of <i>n</i> -Octanol/Water Partition Coefficients (log <mml:math) 0="" 10<="" etqq0="" overlock="" rgbt="" td="" tj=""><td>Tf 50 477</td><td>Td (xmlns:n</td></mml:math)>	Tf 50 477	Td (xmlns:n
278	of Polychlorinated Biphenyls by Using Quantum Chemical Descriptors and Partial Least Squares. Journal of Chemistry, 2013, 2013, 1-8.	1.9	10
279	Uptake and Distribution of Cd in Sweet Maize Grown on Contaminated Soils: A Field-Scale Study. Bioinorganic Chemistry and Applications, 2013, 2013, 1-8.	4.1	27
280	Influence of ferric iron on the electrochemical behavior of pyrite. Ionics, 2011, 17, 169-176.	2.4	41
281	Arsenic speciation in turnip as affected by application of chicken manure bearing roxarsone and its metabolites. Plant and Soil, 2009, 316, 117-124.	3.7	44
282	Estimation of Water Solubility of Polycyclic Aromatic Hydrocarbons Using Quantum Chemical Descriptors and Partial Least Squares. QSAR and Combinatorial Science, 2008, 27, 618-626.	1.4	32
283	Estimation of n-octanol/water partition coefficients of polycyclic aromatic hydrocarbons by quantum chemical descriptors. Open Chemistry, 2008, 6, 310-318.	1.9	9